RESEARCH ARTICLE OPEN ACCESS

Nuclear stiffness through lamin A/C overexpression differentially modulates chromosomal instability biomarkers

Mireia Bosch-Calvet[1,2] | Alejandro Pérez-Venteo[1,2] | Alex Cebria-Xart[3,4] | Marta Garcia-Cajide[1,2] | Caroline Mauvezin[1,2]

[1]Departament de Biomedicina, Facultat de Medicina i Ciències de la Salut, Universitat de Barcelona, Barcelona, Spain | [2]Institut d'Investigacions Biomèdiques August Pi i Sunyer (IDIBAPS), Barcelona, Spain | [3]Institut de Recerca Sant Joan de Déu (IRSJD), Barcelona, Spain | [4]Cancer Science Programme, Laboratory of Pediatric Cancer Epigenetics, Institute for Research in Biomedicine (IRB Barcelona), Barcelona, Spain

Correspondence: Caroline Mauvezin (caroline.mauvezin@ub.edu)

Received: 9 August 2024 | **Accepted:** 22 January 2025

Funding: MBC was supported by fellowship FI (2024 FI-1 00315) from Agència de Gestió d'Ajuts Universitaris i de Recerca (AGAUR) (2024FI-100315; 2021SGR00284). APV was supported by fellowship PREDOC-UB 2022 from the University of Barcelona (PRE2021-098532). ACX was supported by FPI fellowship (PRE2021-098532) from Ministerio de Ciencia, Innovación y Universidades. This study was supported by grants to CM from the Ministerio de Ciencia e Innovación and Agencia Estatal de Investigación (PID2020-118768RJ-I00; AEI/10.13039/501100011033), a Ramon y Cajal fellowship (RYC2022-035576-I) and a research grant from the Asociación Española Contra el Cáncer (AECC; LABAE222994MAUV).

Keywords: autophagy (D001343) | chromosomal Instability (D043171) | lamins (D034882) | lysosomes (D008247)

ABSTRACT

Background Information: Mitosis is crucial for the faithful transmission of genetic material, and disruptions can result in chromosomal instability (CIN), a hallmark of cancer. CIN is a known driver of tumor heterogeneity and anti-cancer drug resistance, thus highlighting the need to assess CIN levels in cancer cells to design effective targeted therapy. While micronuclei are widely recognized as CIN markers, we have recently identified the toroidal nucleus, a novel ring-shaped nuclear phenotype arising as well from chromosome mis-segregation.

Results: Here, we examined whether increasing nuclear envelope stiffness through lamin A/C overexpression could affect the formation of toroidal nuclei and micronuclei. Interestingly, lamin A/C overexpression led to an increase in toroidal nuclei while reducing micronuclei prevalence. We demonstrated that chromatin compaction and nuclear stiffness drive the formation of toroidal nuclei. Furthermore, inhibition of autophagy and lysosomal function elevated the frequency of toroidal nuclei without affecting the number of micronuclei in the whole cell population. We demonstrated that this divergence between the two CIN biomarkers is independent of defects in lamin A processing.

Conclusions and Significance: These findings uncover a complex interplay between nuclear architecture and levels of CIN, advancing our understanding of the mechanisms supporting genomic stability and further contributing to cancer biology.

Mireia Bosch-Calvet, Alejandro Pérez-Venteo, Alex Cebria-Xart and Marta Garcia-Cajide contributed equally to this study.

1 | Introduction

Mitosis ensures the accurate transmission of genetic material across generations. Disruptions in this process can lead to mitotic errors and chromosomal instability (CIN), a hallmark of cancer (Hanahan, 2022, Swanton et al., 2024). Micronuclei, which are extranuclear DNA structures found in daughter cells containing unsegregated chromosome fragments or lagging chromosomes, have historically been used to detect CIN in non-mitotic cells. Micronuclei share structural features with the primary nucleus, including the nuclear envelope (NE), which regulates protein access to the nuclear genome and maintains nuclear-cytosolic separation. The NE is supported by the nuclear lamina, a dense network composed of intermediate filament proteins called lamins. This lamina provides mechanical support, maintaining nuclear shape, stiffness, and integrity, and plays a crucial role in chromatin organization, gene regulation, and DNA replication and transcription (Burke & Stewart, 2013, Butin-Israeli et al., 2015, Dechat et al., 2008, Ovsiannikova et al., 2021). Proper expression and organization of lamins are essential for normal cellular function (Burke & Stewart, 2013, Dechat et al., 2008). Unlike the primary nucleus, micronuclei often exhibit incomplete or defective NE, making them more fragile and prone to rupture (Hatch et al., 2013, He et al., 2019). Indeed, defective nuclear lamina assembly at the micronucleus can impair nuclear pore function or lead to micronuclei disruption, resulting in DNA damage and the activation of innate immune signaling pathways, such as cGAS-STING, which triggers inflammatory responses (de Oliveira Mann & Kranzusch, 2017, Hatch et al., 2013, He et al., 2019, MacKenzie et al., 2017). Interestingly, overexpression of lamins has been shown to prevent micronuclei dysfunction, by potentially stabilizing their NE and promoting their reabsorption into the main nucleus during subsequent mitosis, thus managing CIN levels (Hatch et al., 2013). However, micronuclei can also arise from non-mitotic processes such as DNA damage or mechanical stress, broadening their relevance beyond mitosis. Recent studies highlight their active role in cellular responses to genotoxic stress, indicating that the formation of micronuclei is not only a byproduct of mitotic errors (Fenech et al., 2020, MacDonald et al., 2024). While micronuclei are well-established biomarkers of CIN, they might not be the sole indicators, and the identification of additional biomarkers is crucial for advancing our understanding of CIN and its broader implications for cancer research.

Complementary to the micronuclei, we have recently characterized the toroidal nucleus, a ring-shaped nuclear phenotype, as a novel CIN biomarker (Figure 1A) (Almacellas & Mauvezin, 2022, Almacellas et al., 2021, Pons et al., 2022). The toroidal nucleus also results from mitotic chromosome mis-segregation and can appear in one or both daughter cells (Almacellas et al., 2021). Previous studies demonstrated that lamin B1 and lamin A/C correctly decorate the toroidal nucleus, and that NE reformation precedes toroidal nucleus formation, suggesting that this ring-shaped phenotype does not arise from lamin-associated NE defects (Almacellas et al., 2021). Other studies have observed an enrichment of toroidal nuclei upon treatment with farnesyltransferase inhibitors (FTIs) and in conjunction with centrosome and mitotic spindle defects (Naso et al., 2020, Verstraeten et al., 2011). FTI are a class of targeted therapeutics that inhibit the enzymatic activity of farnesyltransferase, an enzyme crucial for the post-translational modification of proteins, including those involved in cell signaling and cancer progression. In particular, FTI inhibit the farnesylation of lamins, which was shown to modify nuclear morphology. Interestingly, the effect of FTI on toroidal nucleus formation has been shown to differ across cell types, reflecting cell-specific responses to defective lamina processing (Almacellas et al., 2021, Verstraeten et al., 2011). In contrast, one of the cellular stressors shown to significantly induce the formation of toroidal nucleus in several cancer cell lines is the inhibition of autophagy and lysosomal function during mitotic progression (Almacellas et al., 2021). Autophagic vesicles and lysosomes are catabolic compartments involved in the degradation of damaged organelles or dysfunctional proteins and play an essential role in the maintenance of cellular homeostasis (Debnath et al., 2023, Klionsky et al., 2021). The role of autophagy in mitosis still needs clarification, even though lysosomes have been demonstrated to play a key role in protecting faithful chromosome segregation and mitotic progression (Almacellas et al., 2021, Hämälistö et al., 2020, Mathiassen et al., 2017). The inhibition of autophagy induces chromosome mis-segregation and later the formation of toroidal nuclei, however, little is known about its interconnection with nuclear architecture and morphology. Here, we investigated the effects of lamin A/C overexpression on nuclear morphology, specifically focusing on its role in the formation of toroidal nuclei and micronuclei. We sought to determine whether increased lamin levels, known to enhance nuclear stiffness (Stephens et al., 2017, Swift et al., 2013), prevent or promote the formation of toroidal nuclei. Our results showed that lamin A/C overexpression stimulated the formation of toroidal nuclei while reducing the prevalence of micronuclei, thus emphasizing the complementarity of these CIN biomarkers and the distinct molecular mechanisms underlying their formation. We also identified that variation in chromatin compaction and nuclear organization are key factors in the induction of toroidal nuclei. Furthermore, inhibition of the autophagy-lysosome compartment increased the frequency of toroidal nuclei without affecting micronuclei formation, and this effect was independent of defective lamin A processing. In summary, our findings provide new insights into the complementarity of CIN biomarkers—toroidal nuclei and micronuclei—and highlight the complexity of processes regulating genomic stability. Our study advances our understanding of the interconnection between nuclear architecture and CIN, paving the way for the development of potential cancer detection tools.

2 | Materials and Methods

2.1 | Plasmid Cloning

Lenti-mCherry and lenti-mCherry-LMNA plasmids were generated using the backbone of the lenti-Cas9-Blast (Addgene). This plasmid was digested using *XbaI* and *EcoRI* restriction sites to excise the Cas9 and the backbone was isolated using the QIAquick PCR & Gel Cleanup Kit (QIAgen). The mCherry-LMNA plasmid (Addgene) was used to obtain the coding sequences for mCherry and mCherry-LMNA by PCR, adding the *XbaI* and *EcoRI* restriction sites with customized oligonucleotides. PCR products were subsequently digested with *XbaI* and *EcoRI* (NEB), purified using the MinElute PCR Purification Kit (QIAgen) according to manufacturer's instructions, and ligated to the lentiviral vector following a conventional T4 DNA Ligase (NEB) protocol.

2.2 | Cell Culture and Generation of Transient and Stable Cell Lines

U2OS and HEK293-T cell lines were obtained from American Type Culture Collection (ATCC). Cells were grown in DMEM high glucose (Biowest) (4 mM L-glutamine, 4.5 g/L glucose, 1 mM pyruvate) supplemented with 10% heat-inactivated fetal bovine serum (FBS). Cells were incubated at 37°C, 5% CO_2 and 90%–95% of relative humidity. Specific experimental conditions are indicated in figure legends.

U2OS mCherry-LMNA cells were generated in our laboratory by transfecting mCherry-LMNA plasmid using Lipofectamine 2000 (Invitrogen) diluted in Opti-MEM (GIBCO) following the manufacturer's specifications. To generate U2OS stably expressing mCherry-LMNA, 48 h after transfection cells were selected with G418 (Neomycin, 0.5 mg/mL; Thermofisher) for several days and further sorted with Beckman Coulter MoFlo Astrios separator cytometer. Control cells were transfected with empty vector pCDNA3.1 (Thermofisher Scientific). U2OS GFP-Emerin was obtained by transient transfection of Emerin-pEGFP plasmid (Addgene) using Lipofectamine 2000 as described before. Control cells were transfected with pEGFP-N3 (Clontech).

U2OS mCherry-LMNA^{high} and U2OS mCherry-LMNA^{low} were obtained by lentiviral transduction. For viral production, HEK293T were plate on a 100 mm dish and transfected 20 h later (<50% confluence) with 10 μg of lenti-mCherry or lenti-mCherry-LMNA, 7.5 μg pCMV-δR8.2 (Addgene) and 2.25 μg of VSV-G (Addgene) by $CaCl_2$ standard transfection method. The supernatant containing packaged virus was harvested at 36 and 72 h after transfection, centrifugated, and filtered (0.22 μm). For transduction, U2OS cells were grown in medium containing the non-diluted viral particles collected after two infection cycles (high) and the diluted 1:100 or 1:1000 viral particles after one infection cycle (low). Polybrene was added to a final concentration of 4 μg/mL. Cells were sorted with BD FACSAria Fusion instrument 7 days after transduction.

2.3 | Protein Extraction and Western Blot

Cells lysis was performed using RIPA buffer (10 mM Tris-HCl pH 8.0, 1 mM EDTA pH 8, 1 mM EDTA, 0.5 mM EGTA, 1% Triton X-100, 0.1% sodium deoxycholate, 0.1% SDS, 140 mM NaCl) supplemented with 1:100 protease inhibitor (Roche),1:100 phosphatase 2 and 3 inhibitors (Sigma-Aldrich), and Benzonase (Millipore). Protein concentration was determined using Pierce BCA Protein Assay kit (Thermo Fisher Scientific) and equal amounts of proteins lysates were separated by electrophoresis on 4%–12% precast polyacrylamide gel (Invitrogen) and transferred to nitrocellulose membranes (Amersham) in a semi-dry transfer apparatus (Bio-Rad). Membranes were blocked with 3% BSA (Capricorn) in Tris-buffered saline containing 0.1% Tween-20 (Sigma-Aldrich) for 1 h at room temperature. Incubation of primary antibodies was performed overnight at 4°C in 3% BSA. After three washes in TBS-T, membranes were incubated for 1 h at room temperature with secondary antibodies (1:5000) diluted in 3% BSA. Upon incubation, proteins were detected with Chemidoc Imaging System (Bio-Rad) using enhanced chemiluminescence kit (Amersham).

2.4 | Immunofluorescence

Cells were fixed with 4% paraformaldehyde for 10 min and washed in PBS. Cells were permeabilized (PBS 1×, 20 mM Glycine, 0.1% Triton) for 10 min and then blocked (PBS 1×, 20 mM Glycine, 1% BSA, 0.01% Triton) for 1 h. Next, cells were incubated with primary antibodies for 1 h and washed twice with washing solution (PBS 1×, 20 mM Glycine). Cells were then incubated with secondary antibodies for 45 min, followed by two washes. Coverslips were mounted using Vectashield mounting medium containing DAPI (Vector Laboratories) and Ibidi slides were left in PBS after being DAPI stained (Sigma-Aldrich) for 10 min. All the incubations were performed at room temperature.

2.5 | Image Acquisition and Analysis

Confocal images were acquired using a 63× oil 1.4 NA objective from Carl Zeiss LSM 880 confocal microscope and ZEN black software. For toroidal nucleus, micronuclei, and mitotic errors quantification, confocal images were acquired using Opera Phenix High-Content Screening System (PerkinElmer) microscope with a 40× water. Image analysis was performed using Cell counter plugin from FIJI ImageJ software or custom ImageJ macros. Pearson's correlation coefficient was calculated using FIJI ImageJ plugin Intensity Correlation Analysis.

2.6 | Data and Statistical Analysis

Data was analyzed using Excel, RStudio (2024.09.0+375) and GraphPad Prism10 software. Results are presented as Mean ± Standard Deviation (error bars). Replicates are represented as (n) for each independent experiment and consisted in the analysis of a minimum of 200 cells per condition in each experiment. Experimental data sets were compared by unpaired two-sample two-tailed Student's t-test. The figures were edited and assembled using Inkscape.

All materials used in this study are reported in Table 1.

3 | Results

3.1 | Lamin A/C Overexpression Differentially Modulated the Frequency of CIN Biomarkers

The toroidal nucleus is an atypical primary nucleus shaped as a ring, in which the contact sites with cytosolic components are enhanced (Figure 1A). We demonstrated that lamin A/C and lamin B1 properly decorate the toroidal nucleus, and that this phenotype is distinctly marked by the recruitment of lamin A/C surrounding the void (Figure 1B) (Almacellas et al., 2021). It is important to note that some nuclei stained with DAPI may appear similar to toroidal nuclei, which can potentially lead to misidentification. However, the presence of lamin A/C outlining the void serves as a definitive marker to distinguish and accurately identify a toroidal nucleus (Figure S1A, compare toroidal nuclei with normal nuclei). Given the role of the nuclear lamina in providing mechanical support and stability to the NE, here we investigated how lamin A/C overexpression would impact the frequency of

TABLE 1 | List of reagents and materials used in this study.

Experimental Models		
Name	**Source**	**Reference**
HEK293-T	ATCC	CRL-11268
U2OS	ATCC	HTB-96
U2OS mCherry-LMNA^{stable}	In this study	N/A
U2OS mCherry-LMNA^{High}	In this study	N/A
U2OS mCherry-LMNA^{Low}	In this study	N/A

Recombinant DNA		
Name	**Source**	**Reference**
Emerin-pEGFP	Addgene	#61993 (deposited by Eric Schirmer)
lenti-Cas9-Blast	Addgene	#52962 (deposited by Feng Zhang)
Lenti-mCherry	In this study	N/A
Lenti-mCherry-LMNA	In this study	N/A
mCherry-LMNA	Addgene	#55068 (deposited by Michael Davidson)
pCDNA3.1	Thermo Fisher Scientific	V79020
pCMV-δR8.2	Addgene	#12263 (deposited by Didier Trono)
pEGFP-N3	Clontech	6080-1
VSV-G	Addgene	#8454 (deposited by Bob Weinberg)

Antibodies			
Name	**Source**	**Reference**	**Working Concentration**
Anti-Lamin A/C	Cell signalling Technology	2032T	WB 1/1000
Anti-Lamin A/C	Abcam	ab216074	IF 1/300
Anti-LC3	MBL International	pm036	WB 1/1000
Anti-mouse Ig HRP	Thermo Fisher Scientific	A16072	WB 1/10000
Anti-rabbit Ig HRP	Thermo Fisher Scientific	A16104	WB 1/10000
Anti-SQSTM1/p62	MBL International	M162-3	WB 1/1000
Anti-β-actin	Sigma-Aldrich	A2228	WB 1/10000
Goat anti-rabbit IgG-AF647	Thermo Fisher Scientific	A21244	IF 1/400

Oligonucleotides		
Name	**Source**	**Sequence 5' - 3'**
GADPH FWD	Merck	CTCCTCCTGTTCGACAGTCA
GAPDPH REV	Merck	CGGTGCCATGGAATTTGCC
LMNA FWD	Merck	CAGCAGCTTCTCACAGCACG
LMNA REV	Merck	TGCCCATGGACTGGTCCTCA
mCherry FWD	Integrated DNA Technologies	ATGCATCTAGATCGCCACCA TGGTGAGCAA

(Continues)

TABLE 1 | (Continued)

Oligonucleotides		
Name	**Source**	**Sequence 5' - 3'**
mCherry REV	Integrated DNA Technologies	CCTGCTCGACATG*ATCAG GCCCTTAAGACTGA
mCherry-LMNA FWD	Integrated DNA Technologies	ATGCATCTAGATCGCCACCA TGGTGAGCAA
mCherry-LMNA REV	Integrated DNA Technologies	CGTCGTAGTACATTCCTAG GTGGCCTTAAGACTGA

Chemicals, enzymes and other reagents			
Name	**Source**	**Reference**	**Working Concentration**
Benzonase	Millipore	71205-M	50U/mL
BSA	Capricorn	BSA-DG	1–3%
Chloroquine	Sigma-Aldrich	C6628	10 nM
Concanamycin A	Santa Cruz Biotechnology	SC-20211A	10 μM
DAPI	Sigma-Aldrich	D9542	300 nM
DMEM	Biowest	L0105-500	N/A
ECL	Amersham	RPN2236	N/A
EcoRI-HF	New England Biolabs (NEB	R3101S	N/A
EDTA	Sigma-Aldrich	E5134	1 mM
EGTA	Sigma-Aldrich	E4378	0.5 mM
FBS	Diagnovum	D016-500ML	0.1
G418	Thermo Fisher Scientific	11811023	0.5 mg/mL
Glycine	Sigma-Aldrich	G8898	20 mM
GoTaq qPCR master mix	Promega	A6002	N/A
L744832 (FTI)	Sigma-Aldrich	422720	10 μM
Lipofectamine 2000	Thermo Fisher Scientific	11668030	N/A
Methylstat	Medchem	Methylstat	5 μM
NaCl	Sigma-Aldrich	S7653	140 mM
Optimem	Gibco	11058021	N/A
Paraformaldehyde	Sigma-Aldrich	P61148	4%
Phosphatase inhibitor 2	Sigma-Aldrich	P5726	1:100
Phosphatase inhibitor 3	Sigma-Aldrich	P0044	1:100
Protease Inhibitor	Roche	4693159001	1:100
SAHA (Vorinostat)	Medchem	HY-10221	5 μM
SDS	Scharlau	SO04500500	0.1%
Sodium Deoxycholate	Sigma-Aldrich	D5670-5G	0.1%
T4 DNA Ligase	New England Biolabs (NEB)	M0202	N/A
Tris	Serva	37190.03	10 mM
Triton X-100	Sigma-Aldrich	93443	0.1-1%
Trypsin	Gibco	15400-054	1X

(Continues)

TABLE 1 | (Continued)

Chemicals, enzymes and other reagents			
Name	**Source**	**Reference**	**Working Concentration**
Tween 20	Sigma-Aldrich	P7949	0.1%
Vectashield with DAPI	Vector Laboratories	H-2000	N/A
XbaI	New England Biolab (NEB)	R0145S	N/A
Instrument			
Name	**Source**		
Chemidoc Imaging System	Bio-Rad		
FACSAria Fusion Flow Cytometer	Becton Dickinson		
LightCycler Instrument	Roche		
LSM 880 confocal microscope	Zeiss		
MoFlo Astrios Flow Cytometer	Beckman Coulter		
Opera Phenix High-Content Screening System	Perkin Elmer		
Trans-Blot Turbo Transfer System	Bio-Rad		
Software			
Name	**Source**	**Reference**	
GraphPad Prism10	GraphPad	https://imagej.nih/gov/ij	
FiJi ImageJ	FiJi ImageJ	https://imagej.net	
Inkscape	Inkscape	https://inkscape.org	
Rstudio	Posit	https://posit.co/	
ZEN (black edition)	Zeiss	https://www.zeiss.com/	
Other			
Name	**Source**	**Reference**	
HC cDNA Reverse Transcription kit	Thermo Fisher Scientific	4368814	
minElute PCR Purification Kit	QIAgen	28004	
Nitrocellulose Mebrane	Amersham	10600018	
Pierce BCA Protein Assay Kit	Thermo Fisher Scientific	4823227	
Precast gels	Invitrogen	WG1402BOX	
QIAquick PCR & Gel Cleanup Kit	QIAgen	28506	
RNeasy Mini Kit	QUIAgen	74104	

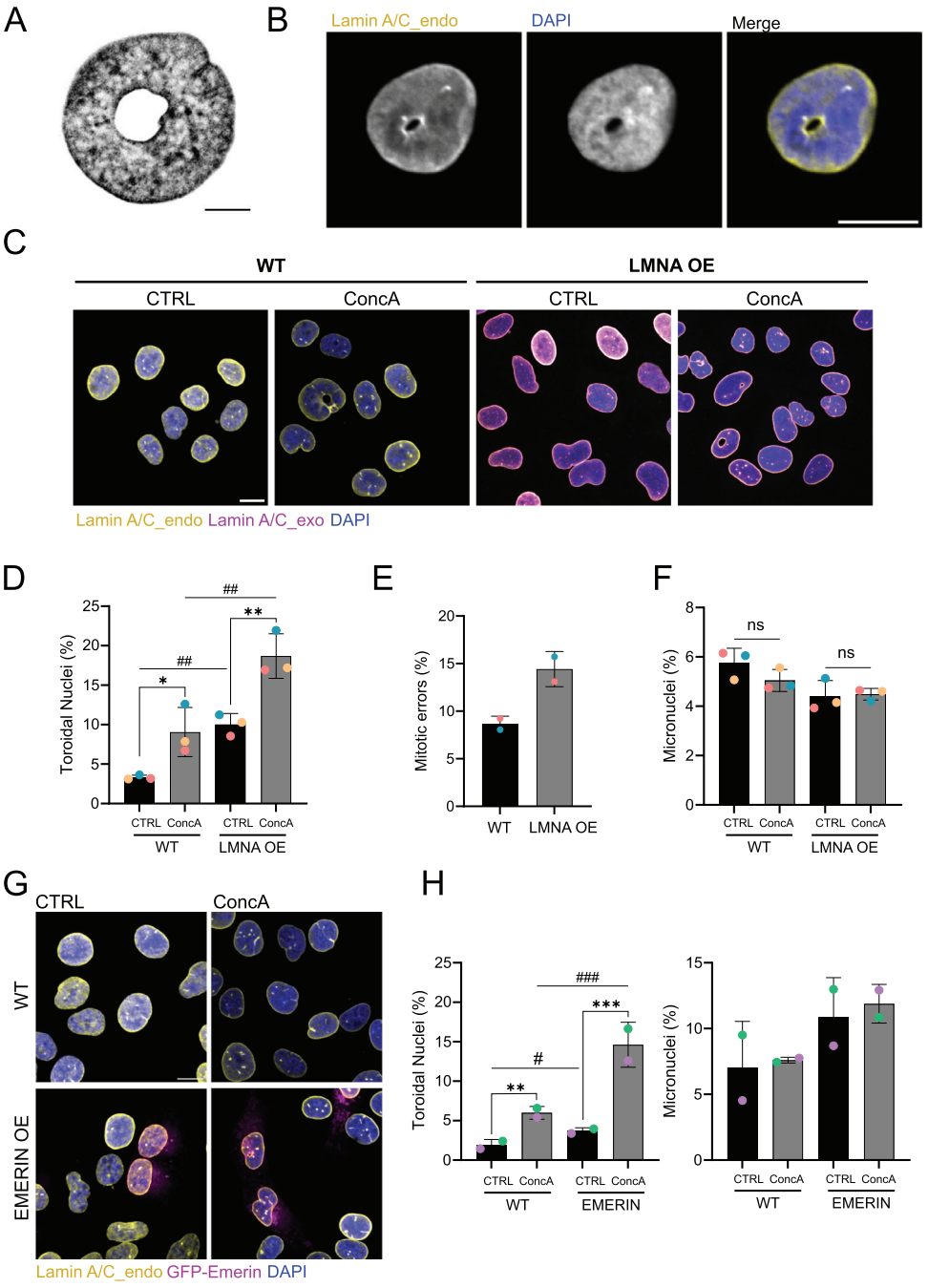

FIGURE 1 | Lamin A/C and Emerin overexpression promote the formation of toroidal nuclei. (A) Representative image of a toroidal nucleus. U2OS cells fixed with PFA and stained with DAPI for DNA detection (gray). Colors were inverted for better visualization. Scale bar: 10 μm. (B) Representative image of a toroidal nucleus decorated with endogenous lamin A/C (yellow). DNA was labelled with DAPI (blue). Scale bar: 10 μm. (C) U2OS WT and U2OS stably overexpressing lamin A/C (mCherry-LMNA, magenta) cells treated or not with ConcA (10 nM) for 24 h, fixed and stained with lamin A/C antibody for endogenous expression (yellow). DNA was stained with DAPI (blue). Scale bar: 10 μm. (D) Quantification of toroidal nuclei frequency (%) in images shown in panel (C). Error bars represent SD of $n = 3$ experiments (20 images/condition, with >20 cells each). (E) Quantification of the percentage of mitotic errors detected in WT and lamin A/C overexpressing cells (LMNA OE) under control conditions. Error bars represent SD of $n = 2$ experiments (>150 images/condition, with >2.000 cells each). (F) Quantification of micronuclei frequency (%) detected in images corresponding to panel (C). Error bars represent SD of $n = 3$ experiments (20 images/condition, with >20 cells each). (G) Representative images of U2OS WT and U2OS overexpressing GFP-Emerin cells (magenta) immunolabelled with lamin A/C antibody (yellow) and treated or not for 24 h with ConcA (10 nM). Nuclei were stained with DAPI (blue). Scale bar: 10 μm. (H) Quantification of toroidal nuclei and micronuclei frequency observed in images from panel (G). Error bars represent SD of $n = 2$ experiments (10 images/condition, with >100 cells each). In panels **D-F, H**, * represents the statistical significance of ConcA-dependent lysosomal inhibition, while # represents the statistical significance of protein overexpression (lamin A/C or Emerin). $^{*}p < 0.05$, $^{**}p < 0.005$, $^{***}p < 0.001$, ns: non-significant; $^{\#}p < 0.05$, $^{\#\#}p < 0.005$, $^{\#\#\#}p < 0.001$, ns: non-significant.

toroidal nuclei. Two plausible hypotheses were envisaged: first, by increasing nuclear stiffness, lamin A/C overexpression could potentially prevent NE deformation and limit the formation of toroidal nuclei; and second, an increase in lamin A/C availability might provide the flexibility required to accommodate such a deformation and allow the nucleus to adopt this toroidal shape more easily. To address this question, we generated U2OS cells stably overexpressing lamin A/C and examined them using confocal microscopy. Wild-type (WT) and lamin A/C-overexpressing cells were treated for 24 h with or without Concanamycin A (ConcA)—a known inhibitor of lysosomal proton pump v-ATPase—, immunolabelled to detect endogenous lamin A/C and stained with DAPI to detect and quantify CIN biomarkers (Figure 1C). Of note, lamin A/C overexpression did not modify lamin A/C distribution and exogenous lamin A/C colocalized perfectly with endogenous lamin A/C under the tested experimental conditions, with Pearson's colocalization coefficient of $r = 0.971$ and $r = 0.956$ for control and ConcA-treated cells, respectively (Figure S1B). Under normal conditions, mCherry-LMNA overexpression led to a 2.85-fold increase in toroidal nuclei prevalence compared to WT cells (Figure 1C,D). ConcA treatment alone caused a 2.59-fold increase in toroidal nuclei frequency in WT cells and the combination of ConcA treatment with lamin A/C overexpression resulted in an additive effect, further exacerbating the frequency of toroidal nuclei beyond the levels observed with either experimental condition alone (Figure 1D). These results indicate that lamin A/C overexpression, rather than reducing CIN, actually promotes the formation of toroidal nuclei and that both proper lysosomal acidification and NE stiffness, mediated by optimal lamin A/C expression, are crucial for preventing toroidal nuclei formation and maintaining genomic stability. Of note, we observed that lamin A/C overexpression induced a significant increase of nuclear area (Figure S1C). Next, we quantified the presence of mitotic errors such as misaligned chromosomes and lagging chromosomes specifically in WT and lamin A/C-overexpressing mitotic cells. Although the mitotic index was comparable between WT and lamin A/C-overexpressing cells (4.77% and 4.35%, respectively) (Figure S1D), cells overexpressing lamin A/C exhibited an altered distribution of mitotic subphases, with a tendency to stall in prophase and telophase (Figure S1E). This suggests a possible mitotic delay, particularly during subphases involving NE breakdown and reformation, indicative of defective mitotic progression. Consistent with this, lamin A/C overexpression increased mitotic errors, thus further correlating impaired chromosome segregation with the presence of toroidal nuclei and reinforcing the toroidal nuclei as CIN biomarker (Figure 1E). Interestingly, these effects observed for toroidal nuclei were not recapitulated when assessing the frequency of micronuclei in the cell populations under the same experimental conditions (Figure 1F). Indeed, lamin A/C overexpression decreased the number of micronuclei, while ConcA-driven inhibition of lysosomal acidification did not modify the frequency of micronuclei in either U2OS WT cells or cells overexpressing lamin A/C (Figure 1F). These results align with prior findings that demonstrated that upregulation of lamin levels reduces the fragility of the NE around micronuclei and promotes their reintegration into the primary nucleus during the subsequent cell division (Hatch et al., 2013). Finally, we further evaluated the effects of the overexpression of Emerin—a known binding partner of lamin A/C in the inner NE (Markiewicz et al., 2006, Popęda et al., 2024, Vaughan et al., 2001). We confirmed that exogenous Emerin was correctly colocalizing with endogenous lamin A/C (Figure S1F). Interestingly, similar to the effects of LMNA overexpression, increased Emerin protein levels also significantly promoted the formation of toroidal nuclei without affecting micronuclei frequency (Figure 1G,H). Overall, our findings provide compelling evidence that increased lamin-dependent NE stiffness promotes CIN, as reflected by a higher frequency of mitotic errors and toroidal nuclei but not micronuclei. The divergences observed in our study between the two CIN biomarkers highlight the importance of further understanding the molecular mechanisms that drive their formation.

3.2 | Variations of Lamin A/C Protein Levels and Chromatin Architecture Trigger the Formation of Toroidal Nuclei

Given the increase in nuclear size in response to lamin A/C overexpression (Figure S1C) and the significant enhanced frequency of toroidal nuclei in these cells, we next investigated whether differential lamin A/C expression would specifically influence the formation of toroidal nuclei. To this end, we generated two additional U2OS cell lines using lentiviral transduction of mCherry-LMNA. These cell lines, named "LMNA^{high}" and "LMNA^{low}", displayed differential lamin A/C expression levels, as confirmed by RT-PCR and western blot analysis (Figure 2A and Figure S2A). While LMNA^{low} cells exhibited reduced lamin A/C expression compared to the stably expressing lamin A/C cells, now renamed "LMNA^{stable}" for clarity, LMNA^{high} cells showed a slight increase of lamin A/C protein levels relative to LMNA^{stable} (Figure 2A). Of note, all three stable cell lines exhibited similar basal autophagy level (LC3-I, Figure 2A). Lamin A/C overexpression resulted in a significant increase in nuclear size compared to WT cells, but no differences were observed in between the three lamin A/C-overexpressing cell lines (Figure S2B). Interestingly, under control conditions, all three lamin A/C-overexpressing cell lines displayed a similar 2-fold increase in toroidal nuclei compared to WT cells, regardless of lamin A/C protein abundance (Figure 2B). This suggests that perhaps a plateau of toroidal nuclei formation has already been reached in LMNA^{low} cells. Next, we confirmed that ConcA treatment significantly enhanced the frequency of toroidal nuclei in WT cells, as well as the additive effect of ConcA-dependent inhibition of lysosomal acidification and lamin A/C-driven nuclear stiffness observed in lamin A/C-overexpressing cells (Figure 2B). Notably, this additive effect was independent of lamin A/C protein levels (Figure 2B). Our results suggest that the concentration of lamin A/C at the NE is a critical determinant of toroidal nucleus formation.

Due to the fact that the status of nuclear lamina is closely interconnected with chromatin compaction levels, and both are determinants of nuclear architecture and stiffness, we further investigated whether modification of chromatin compaction could influence the formation of toroidal nuclei. Understanding their interplay is important as it can impact chromatin dynamics, which may in turn affect nuclear morphology. To this end, U2OS WT cells were treated with SAHA (Vorinostat)—a potent inhibitor of histone deacetylases that promotes euchromatin formation and chromatin decompaction—or methylstat—a well-characterized inhibitor of histone demethylases known to enhance heterochromatin and nuclear stiffness (Stephens et al.,

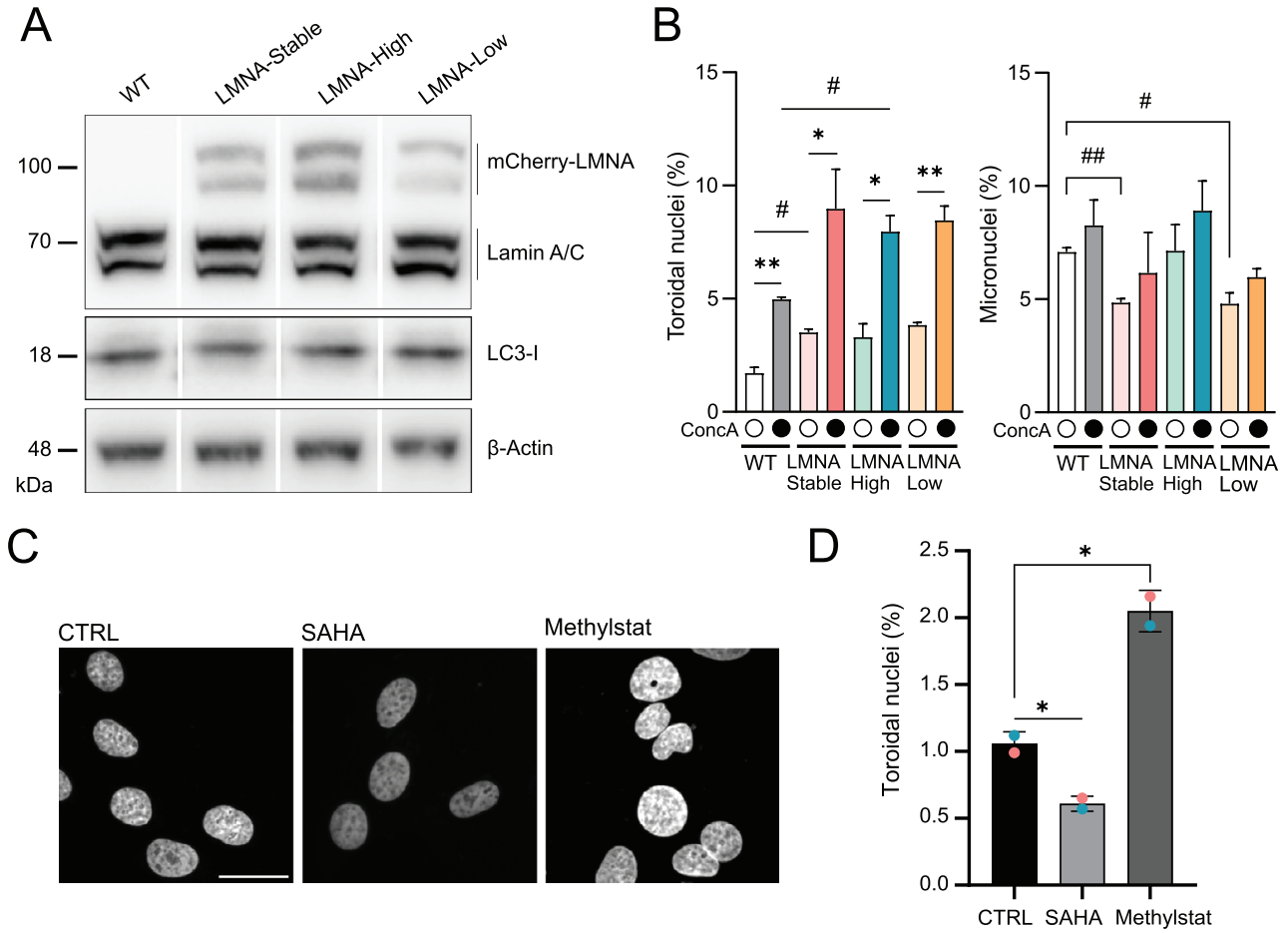

FIGURE 2 | Modulation of lamin A/C expression and chromatin architecture induce the formation of toroidal nuclei. (A) Expression levels of endogenous lamin A/C and overexpressed lamin A/C (mCherry-LMNA, now $LMNA^{stable}$), as well as LC3-I, assessed by western blot in U2OS WT cells and U2OS cells expressing different levels of lamin A/C ($LMNA^{high}$ and $LMNA^{low}$), generated using a lentiviral transduction of mCherry-LMNA. β-Actin used as loading control. (B) Quantification of toroidal nuclei and micronuclei frequency (%) in WT and different lamin A/C overexpressing U2OS cells treated or not with ConcA (10 nM) for 24 h. Error bars represent SD of $n = 2$ experiments (>10 images/condition, with an average of 50 cells each). * represents the statistical significance of ConcA treatment, while # represents the statistical significance of lamin A/C protein overexpression. $^{*}p < 0.05$, $^{**}p < 0.005$; $^{\#}p < 0.05$, $^{\#\#}p < 0.005$. (C) Representative images of U2OS cells treated with SAHA (5 μM) or Methylstat (5 μM) for 24 h, fixed and stained with DAPI for DNA detection. Scale bar: 10 μm. (D) Quantification of toroidal nuclei frequency (%) from images corresponding to panel (C). Error bars represent SD of $n = 2$ experiments (10 images/condition, with >200 cells each) and statistical significance is represented as: $^{*}p < 0.05$.

2018). These treatments, which have opposing effects on chromatin architecture, revealed striking trends. SAHA-treated cells exhibited a reduced frequency of toroidal nuclei, consistent with increased chromatin decompaction and reduced nuclear stiffness (Figure 2C,D). However, it is important to note that SAHA-treated cells presented a distended nuclear phenotype that complicated the quantification of toroidal nuclei and additional studies would be necessary to fully understand the effect of SAHA on the formation of toroidal nuclei. Conversely, methylstat-treated cells displayed a higher frequency of toroidal nuclei, suggesting that chromatin compaction and increased nuclear stiffness favor the adoption of this nuclear phenotype (Figure 2C,D). These findings establish a significant connection between lamin A/C expression levels, chromatin compaction, and the propensity for the formation of toroidal nuclei. Together, our findings underscore the importance of both the composition of the NE and the chromatin state in determining nuclear morphology. Future studies regarding how euchromatin and heterochromatin dynamics influence nuclear stability and CIN biomarker formation would be of interest, as these insights may provide novel therapeutic avenues for targeting chromatin organization in CIN-driven diseases such as cancer.

3.3 | Lamin A/C Maturation Occurred Independently of Autophagy

Previous studies demonstrated that FTIs increase the frequency of toroidal nuclei in HeLa cells, a result not observed in U2OS cells (Almacellas et al., 2021, Verstraeten et al., 2011). FTIs are drugs that target farnesyltransferase, an enzyme that catalyzes the farnesylation of proteins—a post-translational modification involving the addition of a 15-carbon isoprenoid group (farnesyl group) to the C-terminal cysteine residue of certain proteins, including lamin A (Figure 3A) (Rusiñol & Sinensky, 2006, Sinensky et al., 1994). This modification is crucial for the proper localization and function of these proteins, often anchoring them to cell membranes. Lamin A maturation requires farnesylation

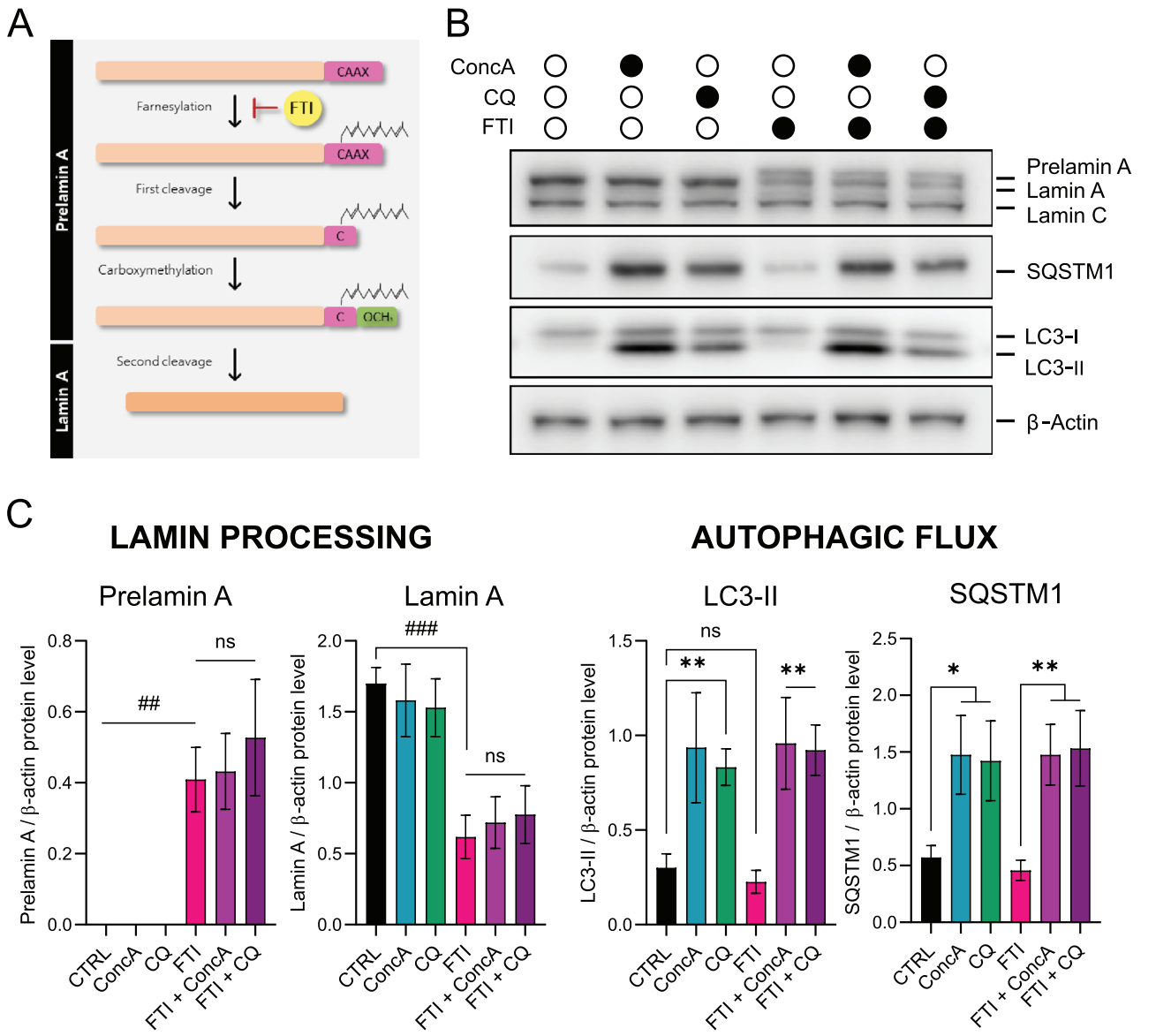

FIGURE 3 | Lamin A processing remains unaffected upon inhibition of the autophagic-lysosomal axis. (A) Schematic representation of prelamin maturation process. FTI induces an accumulation of prelamin A. (B) Representative western blot of U2OS cells treated or not with ConcA (10 nM), CQ (10 μM) or L744832 (FTI, 10 μM) alone or in combination for 24 h. Indicated proteins were analyzed. β-Actin was used as loading control. (C) Quantification of prelamin and lamin A, LC3-II and SQSTM1 protein levels in experimental conditions of panel (B). Protein levels of each corresponding protein of interest were normalized by β-Actin. Error bars represent SD of $n = 3$ experiments and * represents the statistical significance of autophagy inhibition, while # shows the statistical significance of FTI treatment. $^{*}p < 0.05$, $^{**}p < 0.005$, ns: non-significant; $^{\#\#}p < 0.005$, $^{\#\#\#}p < 0.001$, ns: non-significant.

and subsequent processing including serial cleavages (Figure 3A). To better understand the potential link between autophagy inhibition and the increase in toroidal nuclei observed in cells overexpressing lamin A/C (Figure 1C,D), we investigated whether autophagy affects lamin A processing. Cells were treated for 24 h with FTI (10 μM), ConcA (10 nM) or Chloroquine (CQ, 10 μM) — a lysosomotropic drug known to disrupt lysosome acidification — as single or combined treatments. Quantification of autophagic markers protein levels, LC3-II and SQSTM1 (also known as p62), clearly demonstrated the efficiency of both ConcA and CQ to block autophagic flux and to prevent lysosome-dependent degradation of autophagic substrates (Figure 3B,C). On the contrary, FTI showed no effect on the autophagic flux. Our results further demonstrated that neither ConcA nor CQ modified lamin A processing, as no prelamin A band was detected as well as no changes in lamin A or lamin C protein levels (Figure 3B,C). In contrast, FTI treatment resulted in a significant accumulation of prelamin A, as expected (Figure 3B,C). Interestingly, the combination of FTI with autophagy inhibitors did not further induce prelamin A accumulation, indicating that autophagy and lysosomes are not altering lamin A processing. In all, these findings suggest that the processing of lamin A is independent of autophagy, and the observed effects on toroidal nuclei formation upon autophagy inhibition and lamin A/C overexpression are likely due to regulatory mechanisms independent of lamin A farnesylation status and processing.

4 | Discussion

The link between lamin A/C and CIN observed in our study further underscores the significance of nuclear lamina integrity in genomic stability. Our findings showed that overexpression of lamin A/C leads to an increase in toroidal nuclei and a reduction in micronuclei, suggesting that precise regulation of lamin A/C levels is critical for maintaining nuclear integrity and genomic stability. This dual effect highlights the complex role of lamin A/C in nuclear architecture and genome maintenance. Interestingly, our data on the increase of toroidal nuclei is consistent with previous studies in human cancer cells, which have shown that elevated levels of lamin A/C are associated with high-risk cancers and stressful conditions such as CIN (Hatch et al., 2013, Kong et al., 2012). This suggests that a delicate balance in lamin A/C expression is required to avoid the potential consequences of its dysregulation, as seen in laminopathies. Laminopathies are a group of rare genetic disorders caused by mutations in the *LMNA* gene, which encodes the nuclear lamina proteins lamin A and lamin C. In laminopathies, the defective nuclear lamina compromises the mechanical stability of the nucleus, making cells more susceptible to mechanical stress and leading to abnormal nuclear morphology. This aberrant nuclear architecture can disrupt chromatin organization and impair DNA repair mechanisms, contributing to increased CIN and cellular dysfunction involved in a wide spectrum of diseases, including muscular dystrophies, cardiomyopathies, lipodystrophies, and premature aging syndromes such as Hutchinson–Gilford Progeria Syndrome (HGPS). Interestingly, it has been previously shown that nuclear shape is differentially affected by the loss of lamin A or lamin C, where loss of lamin A preferentially increased nuclear blebbing (Pho et al., 2024). It would be of significant interest to investigate the prevalence of toroidal nuclei and micronuclei in laminopathy models to further study the link between lamin levels and CIN. Such investigations could provide deeper insights into how lamin A/C dysregulation impacts nuclear stability and genome integrity across different pathological contexts.

In addition to their well-established role in providing mechanical support to the NE, lamins, particularly lamin A/C, also influence other critical cellular processes such as peripheral chromatin tethering and gene expression. Lamin A/C interacts with the nuclear lamina to anchor peripheral chromatin, which is crucial for maintaining chromatin organization and regulating gene expression (Burke & Stewart, 2013, Buxboim et al., 2023, Madsen-Østerbye et al., 2023, Shevelyov, 2023). This tethering plays a key role in processes such as DNA replication, DNA damage repair, and the regulation of transcription, all of which can impact nuclear morphology (Butin-Israeli et al., 2015, Herr et al., 2024, Kovacs et al., 2023, Maynard et al., 2019). Thus, while our study focuses on the structural scaffold role of lamins in promoting toroidal nucleus formation, it is important to recognize that their effects on chromatin organization and gene regulation may also contribute to the observed toroidal nuclei. Recent studies have suggested that N-terminal tagging of lamin A/C disrupts its localization at the NE and therefore impeding its function as structural support for the nucleus (Odell & Lammerding, 2024). However, in this study we observed that exogenous lamin A/C exhibited a normal nuclear localization, and colocalized with endogenous lamin A/C. Additionally, GFP-Emerin was also properly localized at the NE. Further experiments would be required to determine whether those differences are cell-type specific or influenced by other mechanisms inherent to cancer cells. Interestingly, modulation of chromatin compaction influences the prevalence of the formation of toroidal nuclei, with more heterochromatin favoring the induction of toroidal nuclei. Further investigations directly mimicking the structural scaffold function of lamin through mechanical or other physical means would help to disentangle the mechanical and non-mechanical roles of lamins and better understand how these functions are involved in the maintenance of nuclear integrity and shape.

Previous studies stated that autophagy is involved in the degradation of nuclear lamina, which could be directly linked to variations in nuclear morphology (Dou et al., 2015, Kim, 2023). Our findings demonstrated that lysosomal acidification blockade in cells overexpressing lamin A/C showed an additive effect on the population of toroidal nuclei. To explore whether inhibition of lamin A processing or autophagy could be interrelated, we studied the impact of these processes. Interestingly, autophagy inhibition did not alter lamin A processing, nor did FTI treatment affect autophagic flux. This suggests that these two processes are independent. Thus, the observed additive effect might be explained by currently undefined mechanisms, and further experiments are needed to clarify this possible synergism. Future studies should focus on identifying these mechanisms and understanding how autophagy could interact with lamin A/C dynamics and NE integrity.

Additionally, the differential impact on CIN biomarkers—where lamin A/C overexpression reduced micronuclei but increased toroidal nuclei—indicates that these biomarkers may be governed by distinct pathways. This divergence highlights the need for a more precise understanding of the factors that trigger chromosome mis-segregation and the formation of specific nuclear phenotypes to be used to mark chromosomally unstable cells. This would be highly relevant for cancer research, as recent work has demonstrated that the nature of the trigger for micronuclei formation significantly influences the subsequent cellular response and the fate of the micronucleated cell (Takaki et al., 2024). Further research aiming at elucidating the specific conditions and the molecular interactions that promote either toroidal nucleus or micronucleus formation would be of interest.

In summary, our study emphasizes the crucial role of lamin A/C in maintaining nuclear integrity and architecture, and its complex involvement in CIN. While autophagy and lamin A processing appear to operate independently, their interplay during mitosis or in response to cellular stress and nuclear instability warrants further investigation. Our findings provide a foundation for future research aimed at developing therapeutic strategies to modulate both processes to improve chromatin stability in cancer and laminopathies.

Acknowledgments

We want to thank the technical facilities at CCiTUB for cell sorting analysis, fluorescent and confocal microscopy. We also would like to thank Dr. Nuria Ferrandiz (CSIC—University of Salamanca) for sharing reagents. We are thankful to the Women in Autophagy (WIA) community for their support. MBC was supported by fellowship FI (2024 FI-1 00315)

from Agència de Gestió d'Ajuts Universitaris i de Recerca (AGAUR). APV was supported by fellowship PREDOC-UB 2022 from the University of Barcelona. ACX was supported by FPI fellowship (PRE2021-098532) from Ministerio de Ciencia, Innovación y Universidades. This study was supported by grants to CM from the Ministerio de Ciencia e Innovación and Agencia Estatal de Investigación (PID2020-118768RJ-I00; AEI/10.13039/501100011033), a Ramon y Cajal fellowship (RYC2022-035576-I) and a research grant from the Asociación Española Contra el Cáncer (AECC; LABAE222994MAUV).

Conflicts of Interest

The authors declare no conflict of interest and no competing financial interests.

References

Swanton, C., Bernard, E., Abbosh, C., André, F., Auwerx, J., Balmain, A. et al. (2024) Embracing cancer complexity: Hallmarks of systemic disease. *Cell*, 187, 1589–1616, https://doi.org/10.1016/j.cell.2024.02.009

Hanahan, D. (2022) Hallmarks of cancer: new dimensions. *Cancer Discovery*, 12, 31–46, https://doi.org/10.1158/2159-8290.CD-21-1059

Burke, B. & Stewart, C.L. (2013) The nuclear lamins: flexibility in function. *Nature Reviews Molecular Cell Biology*, 14, 13–24, https://doi.org/10.1038/nrm3488

Dechat, T., Pfleghaar, K., Sengupta, K., Shimi, T., Shumaker, D.K., Solimando, L. et al. (2008) Nuclear lamins: Major factors in the structural organization and function of the nucleus and chromatin. *Genes and Development*, 22, 832–853, https://doi.org/10.1101/gad.1652708

Butin-Israeli, V., Adam, S.A., Jain, N., Otte, G.L., Neems, D., Wiesmüller, L. et al. (2015) Role of lamin B1 in chromatin instability. *Molecular and Cellular Biology*, 35, 884–898, https://doi.org/10.1128/mcb.01145-14

Ovsiannikova, N.L., Lavrushkina, SV., Ivanova, AV., Mazina, L.M., Zhironkina, O.A. & Kireev, I.I. (2021) Lamin A as a determinant of mechanical properties of the cell nucleus in health and disease. *Biochemistry*, 86, 1288–1300, https://doi.org/10.1134/S0006297921100102

Hatch, E.M., Fischer, A.H., Deerinck, T.J. & Hetzer, M.W. (2013) Catastrophic nuclear envelope collapse in cancer cell micronuclei. *Cell*, 154, 47, https://doi.org/10.1016/j.cell.2013.06.007

He, B., Gnawali, N., Hinman, A.W., Mattingly, A.J., Osimani, A. & Cimini, D. (2019) Chromosomes missegregated into micronuclei contribute to chromosomal instability by missegregating at the next division. *Oncotarget*, 10(28), 2660–2674.

de Oliveira Mann, C.C. & Kranzusch, P.J. (2017) cGAS conducts micronuclei DNA surveillance. *Trends in Cell Biology*, 27, 697–698, https://doi.org/10.1016/j.tcb.2017.08.007

MacKenzie, K.J., Carroll, P., Martin, C.A., Murina, O., Fluteau, A., Simpson, D.J. et al. (2017) CGAS surveillance of micronuclei links genome instability to innate immunity. *Nature*, 548, 461–465, https://doi.org/10.1038/nature23449

MacDonald, K.M., Khan, S., Lin, B., Hurren, R., Schimmer, A.D., Kislinger, T. et al. (2024) The proteomic landscape of genotoxic stress-induced micronuclei. *Molecular Cell*, 84, 1377–1391.e6, https://doi.org/10.1016/j.molcel.2024.02.001

Fenech, M., Knasmueller, S., Bolognesi, C., Holland, N., Bonassi, S. & Kirsch-Volders, M. (2020) Micronuclei as biomarkers of DNA damage, aneuploidy, inducers of chromosomal hypermutation and as sources of pro-inflammatory DNA in humans. *Mutation Research—Reviews in Mutation Research*, 786, 108342, https://doi.org/10.1016/j.mrrev.2020.108342

Almacellas, E., Pelletier, J., Day, C., Ambrosio, S., Tauler, A. & Mauvezin, C. (2021) Lysosomal degradation ensures accurate chromosomal segregation to prevent chromosomal instability. *Autophagy*, 17, 796–813, https://doi.org/10.1080/15548627.2020.1764727

Almacellas, E. & Mauvezin, C. (2022) Emerging roles of mitotic autophagy. *Journal of Cell Science*, 135, jcs255802, https://doi.org/10.1242/jcs.255802

Pons, C., Almacellas, E., Tauler, A. & Mauvezin, C. (2022) Detection of nuclear biomarkers for chromosomal instability. *Methods in Molecular Biology*, 2445, 117–125, https://doi.org/10.1007/978-1-0716-2071-7_8

Naso, F.D., Sterbini, V., Crecca, E., Asteriti, I.A., Russo, A.D., Giubettini, M. et al. (2020) Excess TPX2 interferes with microtubule disassembly and nuclei reformation at mitotic exit. *Cells*, 9, 374, https://doi.org/10.3390/cells9020374

Verstraeten, V., Peckham, L.A., Olive, M., Capell, B.C., Collins, F.S., Nabel, E.G. et al. (2011) Protein farnesylation inhibitors cause donut-shaped cell nuclei attributable to a centrosome separation defect. *Proceedings of the National Academy of Sciences of the United States of America*, 108, 4997–5002, https://doi.org/10.1073/pnas.1019532108

Debnath, J., Gammoh, N. & Ryan, K.M. (2023) Autophagy and autophagy-related pathways in cancer. *Nature Reviews Molecular Cell Biology*, 24, 560–575, https://doi.org/10.1038/s41580-023-00585-z

Klionsky, D.J., Abdel-Aziz, A.K., Abdelfatah, S., Abdellatif, M., Abdoli, A., Abel, S., et al. (2021) Guidelines for the use and interpretation of assays for monitoring autophagy (4th edition)[1]. *Autophagy*, 17, 1–382, https://doi.org/10.1080/15548627.2020.1797280

Hämälistö, S., Stahl, J.L., Favaro, E., Yang, Q., Liu, B., Christoffersen, L. et al. (2020) Spatially and temporally defined lysosomal leakage facilitates mitotic chromosome segregation. *Nature Communications*, 11, 229, https://doi.org/10.1038/s41467-019-14009-0

Mathiassen, S.G., De Zio, D. & Cecconi, F. (2017) Autophagy and the cell cycle: a complex landscape. *Frontiers in Oncology*, 7, 51, https://doi.org/10.3389/fonc.2017.00051

Swift, J., Ivanovska, I.L., Buxboim, A., Harada, T., Dingal, P., Pinter, J. et al. (2013) Nuclear lamin-A scales with tissue stiffness and enhances matrix-directed differentiation. *Science (1979)*, 341, 1240104, https://doi.org/10.1126/science.1240104

Stephens, A.D., Banigan, E.J., Adam, S.A., Goldman, R.D. & Marko, J.F. (2017) Chromatin and lamin a determine two different mechanical response regimes of the cell nucleus. *Molecular Biology of the Cell*, 28, 1984–1996, https://doi.org/10.1091/mbc.E16-09-0653

Vaughan, O.A., Alvarez-Reyes, M., Bridger, J.M., Broers, J.L.V., Ramaekers, F.C.S., Wehnert, M., et al. (2001) Both emerin and lamin C depend on lamin A for localization at the nuclear envelope. *Journal of Cell Science*, 114, 2577–2590.

Popęda, M., Kowalski, K., Wenta, T., Beznoussenko, G.V., Rychłowski, M., Mironov, A., et al. (2024) Emerin mislocalization during chromatin bridge resolution can drive prostate cancer cell invasiveness in a collagen-rich microenvironment. *Experimental & Molecular Medicine*, 56, 2016–2032, https://doi.org/10.1038/s12276-024-01308-w

Markiewicz, E., Tilgner, K., Barker, N., Van De Wetering, M., Clevers, H., Dorobek, M. et al. (2006) The inner nuclear membrane protein Emerin regulates β-catenin activity by restricting its accumulation in the nucleus. *EMBO Journal*, 25, 3275–3285, https://doi.org/10.1038/sj.emboj.7601230

Stephens, A.D., Liu, P.Z., Banigan, E.J., Almassalha, L.M., Backman, V., Adam, S.A. et al. (2018) Chromatin histone modifications and rigidity affect nuclear morphology independent of lamins. *Molecular Biology of the Cell*, 29, 220–233, https://doi.org/10.1091/mbc.E17-06-0410

Rusiñol, A.E. & Sinensky, M.S. (2006) Farnesylated lamins, progeroid syndromes and farnesyl transferase inhibitors. *Journal of Cell Science*, 119, 3265–3272, https://doi.org/10.1242/jcs.03156

Sinensky, M., Fantle, K., Trujillo, M., McLain, T., Kupfer, A. & Dalton, M. (1994) The processing pathway of prelamin A. *Journal of Cell Science*, 107, 61–67, https://doi.org/10.1242/jcs.107.1.61

Kong, L., Schäfer, G., Bu, H., Zhang, Y., Zhang, Y. & Klocker, H. (2012) Lamin A/C protein is overexpressed in tissue-invading prostate cancer and promotes prostate cancer cell growth, migration and invasion through

the PI3K/AKT/PTEN pathway. *Carcinogenesis*, 33, 751–759, https://doi.org/10.1093/carcin/bgs022

Pho, M., Berrada, Y., Gunda, A. & Stephens, A.D. (2024) Nuclear shape is affected differentially by loss of lamin A, lamin C, or both lamin A and C. *microPublication Biology*, https://doi.org/10.17912/micropub.biology.001103.

Madsen-Østerbye, J., Abdelhalim, M., Pickering, S.H. & Collas, P. (2023) Gene regulatory interactions at lamina-associated domains. *Genes*, 14, 334, https://doi.org/10.3390/genes14020334

Buxboim, A., Kronenberg-Tenga, R., Salajkova, S., Avidan, N., Shahak, H., Thurston, A. et al. (2023) Scaffold, mechanics and functions of nuclear lamins. *FEBS Letters*, 597, 2791–2805, https://doi.org/10.1002/1873-3468.14750

Shevelyov, Y.Y. (2023) Interactions of Chromatin with the nuclear lamina and nuclear pore complexes. *International Journal of Molecular Sciences*, 24, 15771, https://doi.org/10.3390/ijms242115771

Kovacs, M.T., Vallette, M., Wiertsema, P., Dingli, F., Loew, D., Nader, G.P.F. et al. (2023) DNA damage induces nuclear envelope rupture through ATR-mediated phosphorylation of lamin A/C. *Molecular Cell*, 83, 3659–3668.e10, https://doi.org/10.1016/j.molcel.2023.09.023

Maynard, S., Keijzers, G., Akbari, M., Ben, E.M., Hall, A., Morevati, M. et al. (2019) Lamin A/C promotes DNA base excision repair. *Nucleic Acids Research*, 47, 11709–11728, https://doi.org/10.1093/nar/gkz912

Herr, L.M., Schaffer, E.D., Fuchs, K.F., Datta, A. & Brosh, R.M. (2024) Replication stress as a driver of cellular senescence and aging. *Communications Biology*, 7, 616, https://doi.org/10.1038/s42003-024-06263-w

Odell, J. & Lammerding, J. (2024) N-terminal tags impair the ability of lamin A to provide structural support to the nucleus. *Journal of Cell Science*, 137, jcs262207, https://doi.org/10.1242/jcs.262207

Kim, Y. (2023) The impact of altered lamin B1 levels on nuclear lamina structure and function in aging and human diseases. *Current Opinion in Cell Biology*, 85, 102257, https://doi.org/10.1016/J.CEB.2023.102257

Dou, Z., Xu, C., Donahue, G., Shimi, T., Pan, J.A., Zhu, J. et al. (2015) Autophagy mediates degradation of nuclear lamina. *Nature*, 527, 105–109, https://doi.org/10.1038/nature15548

Takaki, T., Millar, R., Hiley, C.T. & Boulton, S.J. (2024) Micronuclei induced by radiation, replication stress, or chromosome segregation errors do not activate cGAS-STING. *Molecular Cell*, 84, 2203–2213.e5, https://doi.org/10.1016/j.molcel.2024.04.017

Supporting Information

Additional supporting information can be found online in the Supporting Information section.